An optical tweezer actuated, nanoaperture-grid based Optofluidic Microscope implementation method

Xin Heng,*[1] Edward Hsiao, [1]Demetri Psaltis, [1,2] and Changhuei Yang [1]

[1] *Department of Electrical Engineering, California Institute of Technology, 1200 E. California Blvd., Pasadena, CA, 91125, USA. Tel: +1 626 3954711, fax: 1 626 395 8475*

[2] *School of Engineering, Ecole Polytechnique Fédérale de Lausanne, EPFL STI IOA LO, BM 4 4102, Station 17, CH-1015, Lausanne, Switzerland. Tel: +41 21 6937795, fax: +41 21 69-3693*

[*] Email: xin@caltech.edu

Abstract: We report a novel grid based Optofluidic Microscope (OFM) method where a closely spaced 2D grid of nanoapertures (diameter = 100 nm, separation = 2.5 µm) provided patterned illumination. We achieved a one-to-one mapping of the light transmissions through the nanoapertures onto a high-speed CCD camera. By optically tweezing a targeted sample across the grid in a controlled fashion and recording the time varying light reception from the nanoapertures, we were able to generate high-resolution images of the sample. The achievable resolution limit of the prototype was ~ 110 nm (Sparrow's criterion) under optimal conditions. We demonstrated the technique by imaging polystyrene beads and pollen spores.

© 2007 Optical Society of America

OCIS codes: (110.0110) Imaging systems; (110.1220) Apertures; (130.0130) Integrated optics

---

References and links

1. X. Heng, D. Erickson, L. R. Baugh, Z. Yaqoob, P. W. Sternberg, D. Psaltis, and C. Yang, "Optofluidic microscopy- a method for implementing a high resolution optical microscope on a chip," Lab Chip **6,** 1274 - 1276 (2006).
2. X. Q. Cui, X. Heng, W. W. Zhong, P. W. Sternberg, D. Psaltis, and C. H. Yang, "Imaging microorganisms with a high-resolution on-chip optofluidic microscope," *submitted* (2007).
3. B. Hecht, B. Sick, U. P. Wild, V. Deckert, R. Zenobi, O. J. F. Martin, and D. W. Pohl, "Scanning near-field optical microscopy with aperture probes: Fundamentals and applications," J. Chem. Phys. **112**, 7761-7774 (2000).
4. D. Courjon, *Near-field microscopy and near-field optics* (London: Imperial College Press, 2003).
5. A. Ashkin, J. M. Dziedzic, J. E. Bjorkholm, and S. Chu, "Observation of a single beam gradient force optical trap for dielectric particles," Opt. Lett. **11**, 288-290 (1986).
6. J. Enger, M. Goksor, K. Ramser, P. Hagberg, and D. Hanstorp, "Optical tweezers applied to a microfluidic system," Lab Chip **4,** 196-200 (2004).
7. A. Ashkin, "Forces of a single-beam gradient laser trap on a dielectric sphere in the ray optics regime," Biophys. J. **61**, 569-582 (1992).
8. X. Heng, X. Q. Cui, D. W. Knapp, J. G. Wu, Z. Yaqoob, E. J. McDowell, D. Psaltis, and C. H. Yang, "Characterization of light collection through a subwavelength aperture from a point source," Opt. Express **14**, 10410-10425 (2006).
9. A. T. O'Neil and M. J. Padgett, "Rotational control within optical tweezers by use of a rotating aperture," Opt. Lett. **27**, 743-745 (2002).
10. K. C. Neuman and S. M. Block, "Optical trapping," Review of Scientific Instruments **75**, 2787-2809 (2004).
11. COMSOL_Multiphysics_3.3, in *COMSOL Inc. (http://www.comsol.com/)*.

---

1. Introduction

Recently, our group has developed a new class of imaging systems - the Optofluidic Microscopy (OFM), which combined microfluidic technology and aperture imaging techniques to create compact and cheap microscopes. Target samples were maintained and transported in liquid media in the entire imaging process. The flexibility of the OFM platform

allowed for the use of a wide range of fluid/sample transport mechanisms, such as pressure difference, electrokinetics and optical tweezers. In our previous work [1], we implemented the first OFM prototype based on a linear aperture array and demonstrated imaging of nematode (*C. elegans*) larvae where the primary fluid transport mechanism was pressure difference. A complete on-chip OFM [2] implementation was demonstrated recently and clearly indicated OFM's potential for enabling automated, cheap and compact microscopes and analysis units.

The resolution of an OFM system is fundamentally limited by the aperture size. In some ways, the OFM's imaging strategy share similarities with near field scanning optical microscopy (NSOM) – another aperture based imaging system. In NSOM systems, subwavelength apertures, i.e. nanoapertures, are used as imaging probes in as these tiny nanometric probes can deliver resolution beyond that of conventional microscopes [3, 4]. Commercial NSOM systems are extensively utilized to discover fine structures of chemical, biological or geological samples. However, while the concept of NSOM is simple, NSOM systems, in general, are neither cheap nor fast. During NSOM's image acquisition, the scanning system generally requires sophisticated actuation and feedback control to achieve stable raster scanning. As such, the whole imaging procedure is difficult for a novice and very time consuming. In addition, most commercially available NSOM systems cannot operate in liquid media – a significant impediment to biological studies.

In this paper, we report on OFM implementation that 1) can improve upon the imaging speed of array based OFM systems under specific conditions, and 2) offers a promising way for generating NSOM-type scans more quickly and simply. Some of the key differences from the previous OFM implementation [1] included: 1) The use of nanoapertures as illumination sources rather than light collection units as in the first OFM prototype [1]. 2) Replacement of a linear nanoaperture array with a 2D nanoaperture grid. 3) The use of an optical tweezer to actuate target samples over the nanoaperture grid.

In the following sections, we will first introduce the design of the new OFM prototype and describe its operation. We will then describe the nanoaperture grid in detail. Next, we will report on our implementation and characterization of an optical tweezer with an asymmetric beam profile, which better satisfied our need of a robust sample manipulator. Finally, the experimental results with mulberry pollen spores and polystyrene microspheres will be presented.

2. Methods

2.1 Imaging Method

The experimental scheme is shown in Fig. 1. The optical tweezer implementation in our experiment is depicted in the upper left section of Fig. 1, and the imaging segment of the experiment is shown in the lower half. In brief, the method uses the optical tweezer to trap the target object and actuate it over the nanoaperture grid. The passage of the target across the grid interrupts the light transmitted from the nanoapertures. By measuring the time varying light transmission changes, an image of the target can then be produced.

In the experiment, a white LED light source (Lamina, Titan series, daylight white) illuminated the nanoaperture grid. The transmissions through the nanoapertures were collected by an objective lens (Olympus, 40X, NA = 0.8, water, IR) and imaged onto the recording CCD camera (Princeton Instruments, Spec10-100) with an achromatic camera lens (f= 20.0 cm from Thorlabs). The average diameter of the nanoapertures was 100 nm (as determined by SEM, Fig. 2(c)) and they were spaced 2.5 µm apart from each other. Due to the relatively large spacing, we were able to resolve the light transmissions through each nanoaperture uniquely on the CCD acquired images of the grid.
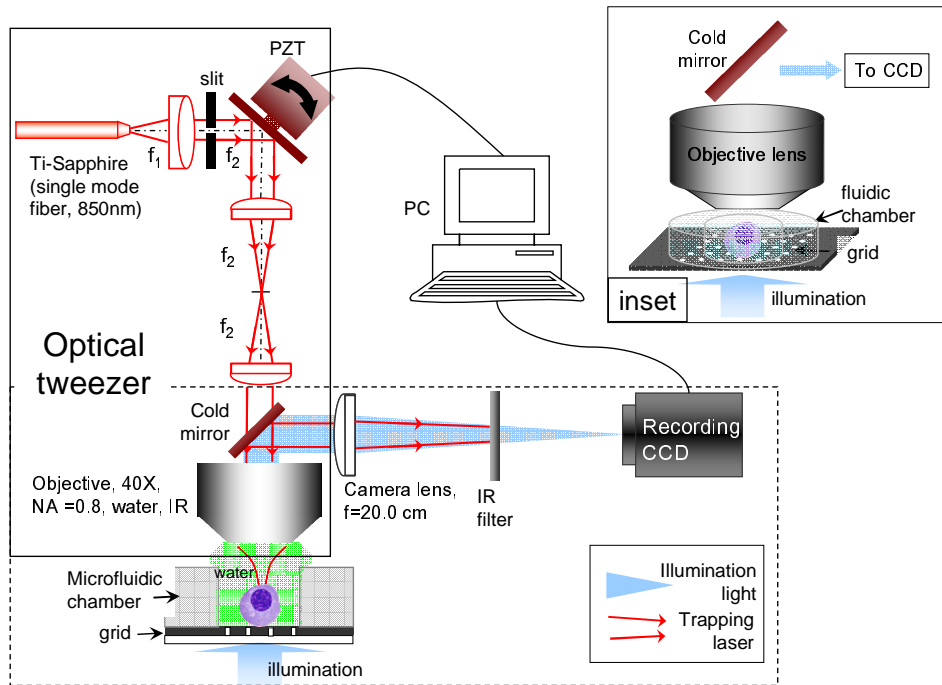
Fig. 1. Illustration of the entire imaging system. Ti-Sapphire: Ti-Sapphire laser (λ= 850 nm). f_1: collimation lens (f_1=3.5 cm). f_2 (2 pieces): 4f scanning system (f_2 = 10.0 cm). PZT: Piezo scanning tube (Physik Instrumente S-334). Cold mirror (R: 400-700 nm, T: 780 nm onward, from Newport). Objective lens: Olympus, 40X, NA=0.8, water, IR. Illumination source: white LED (Lamina, Titan series, daylight white). IR filter: Newport short-pass @ 650 nm. Recording CCD: Princeton Instruments (Spec10-100). Inset: zoom-in image of the Fig. 1 setup showing the 2D nanoaperture grid, its arrangement with the optical tweezer and the fluidic chamber.

Optical tweezer [5] is a mature tool for manipulating micron sized objects, such as single cells. One of its major advantages is that it can easily place and transport cells with excellent accuracy. As such, the optical tweezer is a good fit with the actuation needs of OFM [1] and other microfluidic devices [6]. In our experiment, the optical tweezer used a Ti-Sapphire laser (Spectral Physics Tsunami) operating at 850 nm in cw mode as the light source. The light was coupled into a single-mode fiber, collimated by f_1 (beam diameter = 8 mm) and steered by a PC controlled PZT mirror scanner (Physik Instrumente S-334). A 4f lens relay in the scanning system ensured that the geometric center of the laser beam was always coincident with the center of the back aperture of the microscope objective during scanning. Note that the light components of the trapping beam backscattered from the metallic nanoaperture plate can be strong and can easily saturate the recording camera's CCD pixels. To avoid saturation, a cold mirror (from Newport) and an IR filter (Newport, short wave pass, 650 nm) were introduced into the system to deflect the backscattered components. The power of the trap beam at the exit end of the objective lens was set at 20 mW – a power level that is sufficient for keeping the samples we used firmly trapped and that is tolerable to biological samples.

We note that target samples used in this study have high mass-density (ρ), so that they naturally settled onto the device's floor by gravity. The optical tweezer, although strong enough to trap and translate the samples across the nanoaperture grid, was not strong enough to lift the object of interest from the floor. We verified this point by calculating the levitation

force based on the ray approximation developed by Ashkin [7]. We found that, at an optical tweezing power of 20 mW, the force was too weak to lift the object.

As the target was tweezed across the nanoaperture grid, it interrupted and scattered the light, which caused changes in the signal recorded by the camera. The time varying transmission changes associated with each nanoaperture effectively represented a line scan across the target (see an example, Fig. 5(a)). By choosing to tweeze the target across the nanoapertures at a small tilt angle (θ) with respect to one of the principle axis of the grid (x-axis in Fig. 2(b)), we were assured that the line scans acquired with the nanoapertures overlapped appropriately and fully covered the entire sample- a sufficient-sampling condition.
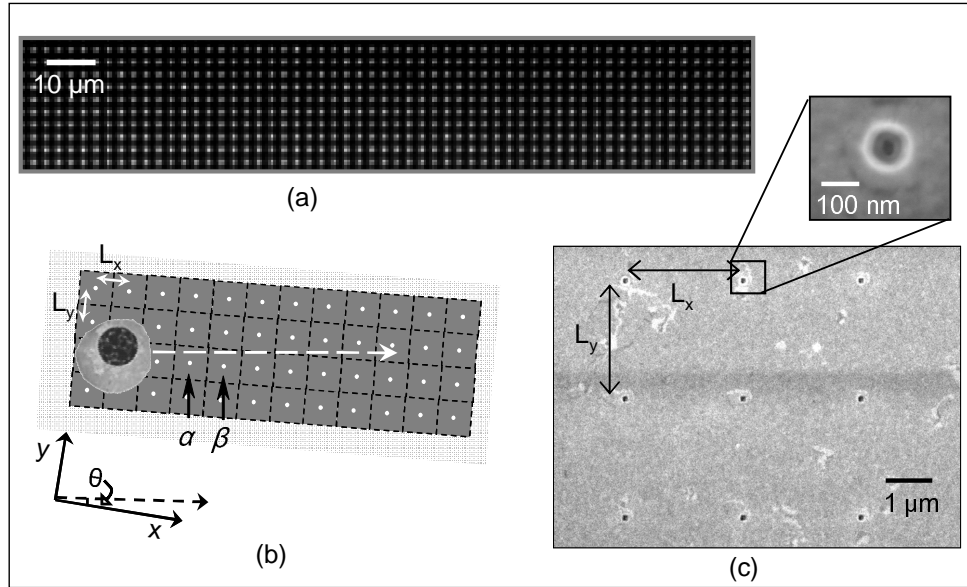

Fig. 2. (a). Image of the 2D nanoaperture grid shown on the recording CCD camera; there is no sample in this region. (b) The orientation of the nanoaperture grid with respect to the scanning direction of the sample. L_x: aperture spacing in x direction; L_y: spacing in y direction; θ: the angle between the scanning direction of the sample and the x-axis. (c) Scanning electron microscope (SEM) image of the nanoaperture grid. The substrate is aluminum. The inset shows one typical nanoaperture (D= 100 nm).

The appropriate composition of the acquired line scans to form an image of the target required knowledge of the spacing between nanoapertures (L_x, L_y in Figs. 2(b) and 2(c)), the target's flow speed (V), and the assurance that the object maintained its shape and orientation during the entire image acquisition process. The composition process was straightforward. For example, nanoaperture α and β in Fig. 2(b) acquired adjacent line scans of the target. As the object passed nanoaperture α before it passed β, the line scan associated with nanoaperture β needs to be time shifted by

$$\Delta t = \frac{L_x \cos\theta}{V}$$

(1)

in order to synchronize with the line scan associated with nanoaperture α.

In general, the time delay factor can be computed from:

$$\Delta t = \frac{L_x \cos\theta}{V}(n-1) - \frac{L_y \sin\theta}{V}(m-1) \qquad (2)$$

where m (or n) is the row (or column) index of the nanoaperture in question.

The pixel density of the final OFM image had the following characteristics. The pixel size in y direction (δy) and that in x direction (δx) can be expressed as follows:

$$\delta y = L_x \sin(\theta)$$
$$\delta x = V \delta t \qquad (3)$$

where δt is the CCD camera time step. In our experiment, we set the scanning speed of the trapped sample at $V = 0.7$ μm/sec, and the camera's frame rate at $\delta t = 0.11$ second/ frame. The tilt angle θ was fine adjusted to be 0.03 in rad. Under this condition, the pixel size δy was ~75 nm and δx was ~80 nm. It is worth noting that the resolution of this system is given by the larger of the following two factors: image's pixel size or the width of the transmission profile associated with the nanoaperture. In our experiment, the second parameter was the larger of the two. The issue of resolution will be further discussed in the Results section.

Nanoaperture grid and the fluidic chamber

The inset of Fig. 1 shows the nanoaperture grid, an open fluidic chamber (diameter = 1mm, thickness = 2 mm) and their orientation with respect to the objective lens.
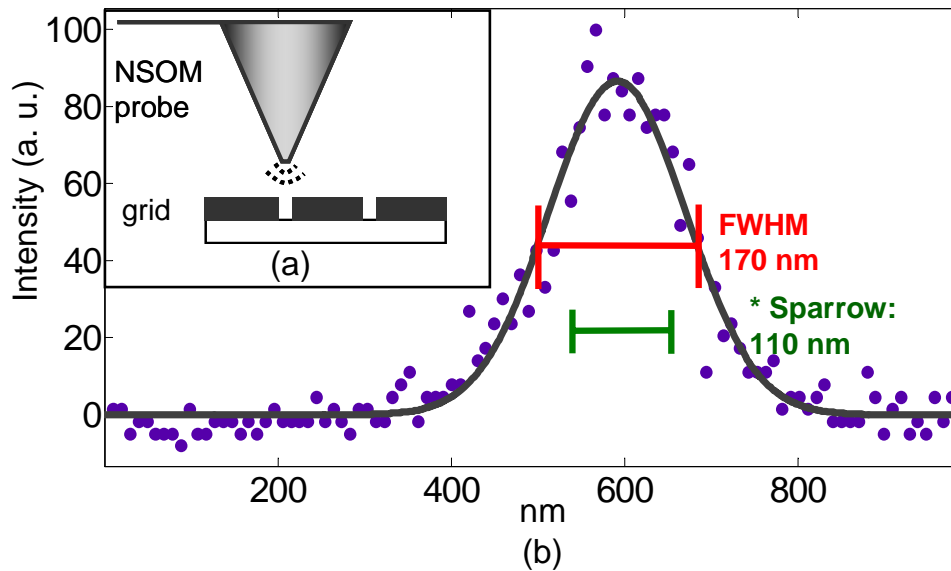

Fig. 3. Measurement of the resolution limit. (a) Illustration of the measurement scheme, where the NSOM probe was taken as a virtual point source. The tip was held in close proximity to the nanoaperture plane. (b) The point-spread-function profile of a typical nanoaperture as measured with the NSOM tip; the width was 170 nm (FWHM, <u>red bar</u>). The dark solid line was a Gaussian fit to the curve of the point spread function. * After accounting for the finite NSOM tip size, the near-field imaging resolution of this nanoaperture was established to be 110 nm (Sparrow's criterion, <u>green bar</u>).

We fabricated the nanoaperture grid using the following procedure. First, a clean quartz wafer was coated with a 100 nm thick layer of aluminum by an electron-beam evaporator (CHA Mark 40). Then a thin layer (250 nm) of PMMA 950 C4 was spun onto the aluminum plate. Next, the aperture grid was patterned on PMMA by a high-resolution electron beam writer (Leica EBPG 5000) and then transferred onto aluminum by a chlorine based reactive ion etcher. Finally, the PMMA residue was completely stripped off by methylene chloride.

In nanoaperture based imaging, the resolution limit of the system is fundamentally determined by the size of the nanoaperture [4, 8]. We performed a resolution check of our system with the help of a commercial NSOM system (WITec alpha-SNOM, tip diameter= 100 nm, λ= 650 nm). The characterization scheme was the same as that presented in a previous paper from our group [8] , and is illustrated in Fig. 3(a). The NSOM tip served as a nanometric test object in this experiment. Figure 3(b) shows the result with a typical nanoaperture. We can see that the point spread function as measured with the NSOM had a FWHM value of 170 nm. By accounting for the finite NSOM tip size (100 nm) and deconvolving its contribution from the measurements, we obtained a near-field resolution of 135 nm (FWHM) or 110 nm (Sparrow's criterion) for the aperture grid. These two values can be taken as good estimates of the resolution limit of this imaging system.

In our earlier experiments, we observed that, for fluidic reservoir that was larger than 2 cm, objects optically trapped in water underwent constant vibrations due to agitation from the surrounding fluid. The standard deviation of the agitation for a 10 µm polystyrene bead was found to be approximately 120 nm. By placing the object within a small fluidic chamber on the order of 1 mm in diameter, jittering of the microsphere was reduced normally by 5 to 10 times, which is sufficiently good for the imaging experiment. Another noteworthy advantage of using a small fluidic reservoir over a large one is that introducing confined fluidic environment dramatically reduces the incidence of undesirable floating objects during data acquisition. Floating objects suspended in the medium can randomly change the light transmission through nanoapertures and introduce undesirable power fluctuations into the system.

Optical tweezer actuation

The OFM imaging method required that the sample maintain the same orientation while passing over the nanoaperture grid. While a standard optical tweezer based on a circular Gaussian beam can firmly trap a sample, the radial symmetry of the trap is not good at preventing target rotation. We overcame this problem by reshaping the laser beam with a slit as shown in Fig. 1. The slit truncated the circular beam and introduced intensity anisotropy at the focal plane. Using this simple method [9], we found that a laser beam profile with a 5:1 aspect ratio was sufficient to suppress the sample rotation during the sample translation. In addition, we observed that a trapped sample (pollen spore) typically aligned with the slit orientation within seconds and the stable trapping condition remained for the entire imaging process (angular rotation of sample did not exceed 0.01rad).

We experimentally verified the robustness of the optical tweezer with the use of 10µm and 1µm polystyrene spheres. The testing scheme was similar to the equipartition method in optical trap characterization [10]. In this test, the optical tweezer was not scanned and the sample was firmly trapped at the origin. The optical trap was then gradually weakened by attenuating the laser beam. The migration of the microsphere from its origin was then used to characterize the strength of the optical trap. From Figs. 4 (a) and 4(b), it can be seen that the microspheres were firmly trapped when the laser power was more than 15 mW. The trap effectiveness began to diminish when the laser power dropped to 10 mW. This experiment informed our decision to set the nominal trapping laser power used in the rest of the experiments at 20 mW.
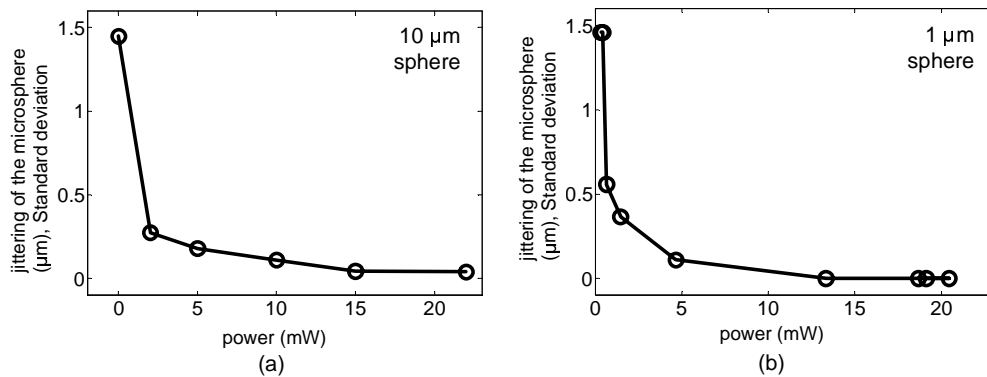
Fig. 4, Strength of the asymmetric optical tweezer. (a) The deviation of the microsphere (diameter =10 µm) away from its origin in the lateral plane. (b) The deviation of the microsphere (diameter =1 µm) away from its origin.

3. Results

We demonstrated the ability of this optical tweezer coupled OFM system by imaging polystyrene beads and paper mulberry pollen spores. Figures 5(e) and 5(f) show OFM images of two paper mulberry pollen spores (Duke Scientific, diameter =11 µm - 17 µm). Figure 5(g) shows an OFM image of a 10µm polystyrene microsphere. Figures 5(b), 5(c), and 5(d) are corresponding images acquired with the home-built imaging system shown in Fig. 1 except that the nanoaperture plate was not used.

It can be clearly seen that the OFM acquired images at this resolution were distinctly different in appearance from the conventional microscope images, especially 'the depth of the images'. This is because the depth of field (DOF) associated with OFM is significantly shorter than that of a conventional microscope. Through a simple diffraction analysis by the finite element methods (COMSOL Multiphysics) [11], we have calculated that the point spread function associated with a typical nanoaperture (D=100 nm, λ= 650 nm) will double in width at a distance of about 120nm away from the nanoaperture plane. On the other hand, the DOF of a conventional microscope can be estimated in the case of Gaussian beam focusing by the same objective lens (40X, NA= 0.8, water, λ=650 nm)). Our calculation shows that the point spread function for the microscope will double in width at a distance of about 1.0 µm from the plane of focus.

To obtain the best resolution with the OFM system, the object needed to be as close to the nanoaperture grid as possible. The blurry edges in some of the OFM images can be attributed to the fact that the edges of the ellipsoidal objects were at appreciable distances from the nanoaperture plane.

The relatively low quality of the periphery of the acquired images can be attributed to the fact the object's edges were insufficiently close to the grid. Going forward, this suggests that target object will need to be intrinsically flat so that the object can make maximal contact with the grid or a means for flattening the object against the grid is needed. Note that such a limitation of nanoaperture based OFM also exists in commercial NSOM and total internal reflection fluorescence microscope (TIRFM).
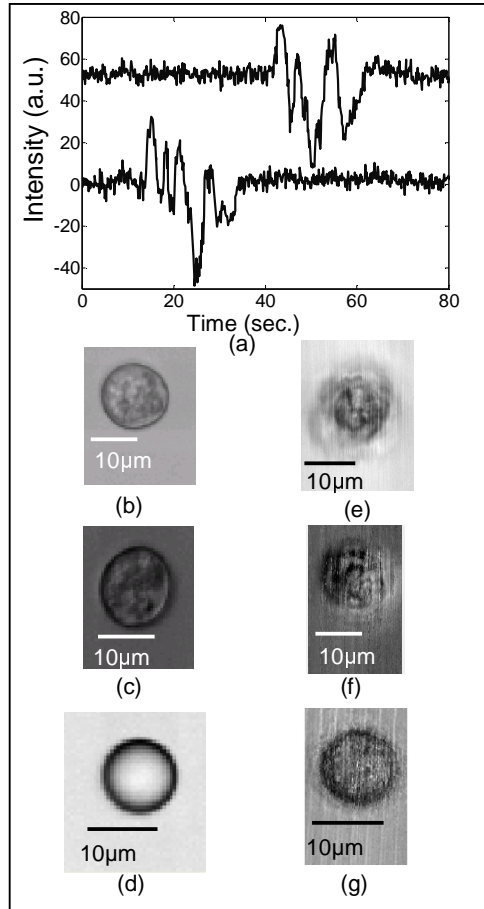
Fig. 5. (a). Example of the transmission time-of-flight traces from two nanoapertures that are in the same row but 25 µm apart; these two apertures scan different segments (0.75 µm apart in y direction) of the sample: a pollen spore. (b, c) Microscope images of two paper mulberry pollen spores. The microscope setup was the same as Fig. 1 except that the nanoaperture plate was removed. (d) Microscope image of a 10µm polystyrene microsphere. (e, f) OFM images of two paper mulberry pollen spores. (g) OFM image of a 10µm microsphere.

4. Discussions

As alluded to previously, this grid based approach can benefit both OFM systems and NSOM systems. In fact, an ultrahigh resolution on-chip implementation will represent a hybrid OFM and NSOM system. This section is divided into two sub-sections. In the first, we will discuss the benefits and tradeoffs of implementing an on-chip grid based OFM system. In the next sub-section, we will examine this technology in the context of NSOM systems.

4.1 Grid based OFM system

There are several significant differences associated with a grid based OFM in comparison with an array based OFM. First, when imaging the same object, a grid-based system can be much shorter than an array-based system. The shortening of the imaging region makes it easier for the flow strategy to satisfy the OFM's requirements, i.e. stable, rotation-free object

transportation during the imaging process. For example, when imaging a cell (diameter, D= 9μm) with an array based OFM (δy =75 nm, Lx= 2.5 μm), the object would need to maintain a constant speed and a steady orientation within a scan range of 300 μm (i.e., D*sin$^{-1}(\theta)$). However, with a grid-based system, the object would only need to remain stable for a distance of about 83 μm (i.e., L_x*sin$^{-1}(\theta)$).). This can be a significant implementation advantage for situations where the target's shape or orientation is particularly susceptible to change – the shorter the scan duration, the less chance of a shape or orientation change ruining the image acquisition process. In addition, even as an off-chip and bulk optical implementation, the grid design is an efficient way to implement simultaneous multiple NSOM scans. On the other hand, the array design is well suited for direct implementation on a linear CCD or CMOS sensor array. The grid design requires the use of a 2D sensor chip.

4.2 Grid based NSOM system

This grid based approach is a simplified implementation design for NSOM systems that is easier to operate. The method brings two advantages in this respect. First, multiple nanoapertures can simultaneously scan the target at the same time – the total number equals the number of nanoapertures the target object overlaps at a given time during the scan. Second, this approach drastically simplifies the scanning pattern: with the grid based OFM, the target object needs only to make a single sweep over the grid, as opposed to a complicated raster scan pattern that a conventional NSOM system employs.

However, we recognize that the path to acquiring high quality NSOM-type images is a long one. Better and more robust means of controlling the samples is required, such that larger portion of a sample can be placed sufficiently close to the nanoapertures. We believe the image quality can be significantly improved by implementing a means to squash the object against the grid. Achieving such a condition without significantly disturbing the functions of the biological objects is not technologically trivial and deserves further investigation.

5. Conclusions

In conclusion, we have presented a new type of OFM systems - nanoaperture-grid based OFM, which is comprised of a 2D nanoaperture grid that functioned as an illumination source, an optical tweezer that translated the target sample over the grid, and a collection system that measured the time varying transmission changes associated with the nanoapertures during the scan. This OFM shared similar image formation mechanism with NSOM and had an experimentally determined resolution limit of 110 nm (Sparrow's criterion). The simplified scan pattern and simultaneous scanning nature of this implementation indicated that this is a simpler and potentially faster scanning replacement for the NSOM for a range of applications. In addition, this paper also reported on the first application of optical tweezer as a sample delivery mechanism for aperture based imaging. By using a moderate laser power, we showed that an asymmetric optical scanner was able to firmly trap and stably transport micron-sized samples. The robustness of the optical tweezer was tested by measuring the deviation of trapped microspheres. We demonstrated the use of this system by acquiring images of polystyrene microspheres and mulberry pollen spores. We note that images acquired through this study were mid-quality and were unable to show the full high resolution potential of this system. There remains the technical challenge of effectively pushing the target objects so that they are flat against the scanning grid.